JOURNAL OF MATERIALS SCIENCE 27 (1992) 4567–4576

Structure–thermomechanical parameters relationship and Zener–Hollomon equation for two vanadium microalloyed steels

C. GARCÍA DE ANDRÉS, M. CARSÍ, M. P. DE ANDRÉS
CENIM, Avda. Gregorio del Amo, 8-28040 Madrid, Spain
F. PEÑALBA
INASMET, Camino de Portuetxe, 12-20009 San Sebastian, Spain

Hot torsion tests were conducted to simulate forging processes in two vanadium microalloyed steels, types 40MVS6 and 30MSiV62, varying both the conditions of test temperature and time as well as the strain and strain-rate conditions, in order to obtain final results comparable to the classic Q + T steels, direct from the forge. The Zener–Hollomon equations were also calculated, indicating the conditions of application which theoretically permit the prediction of forging parameters, in accordance with the needs or possibilities of an industrial plant.

1. Introduction

The 1950s and 1960s saw the commencement of studies aimed at substituting low-carbon steels with microalloyed steels, based on the increases of resistance which were indicated by the Hall–Petch equation and established by the studies of Gensamer, who quantified the structure–parameters relationship. So too in the 1970s and 1980s the possibility of taking advantage of the improvements in mechanical properties produced by microalloy-forming elements has been extended to steels with higher carbon contents, to substitute classic Q + T steels, obtaining similar and, in any case, acceptable results, as well as achieving economy both in raw materials and energy consumption.

The paper studies two microalloyed steels with different carbon contents, with the aim of substituting a classic Q + T steel such as 38C2, widely used in the automobile industry. Thus, a commercial Q + T steel was subjected to a standard forging process, the final results being conditioned by its industrial use, chemical composition and mechanical properties, which are shown in Table I.

Two other commercial, vanadium microalloyed steels were studied, namely 30MSiV62 and 40MVS6, which in principle might offer results comparable to those above, and whose compositions are shown in Table II.

The initial rolling conditions, apart from being imposed by the characteristics of the steels, did not have any effect on the study, given that the aim was to examine the variables of the forging process in microalloyed steels, in order to obtain the same results as those of a standard manufacturing process. That is to say, the characteristics of Q + T steels are predetermined and the objective was to obtain them with microalloyed steels with pre-established rolling by varying the forging parameters. No doubt the optimization of the rolling process might vary the results, but that was not the aim of this study.

In order to attain these objectives, a study had to be made of the variable which, apart from the composition, fundamentally determines the mechanical properties of a microalloyed steel, essentially its elastic limit and transition temperature. According to Gladman *et al.* [1], the grain size and the interlamellar distance contribute most to the final results. As fine a structure as possible had to be obtained, bearing in mind the collateral conditions, maximum ductility for an optimum forging temperature allowing for the dissolution of carbides, nitrides or carbonitrides and thus activating the mechanisms proper to these steels in addition to the real manufacturing conditions.

Lastly, the Zener–Hollomon equation was calculated, which is considered to be the best expression of the state equation of a steel and which allows, within its range of application, for the variation of the thermomechanical treatment conditions, following equivalent cycles.

The torsion tests conducted and detailed in this paper aimed both to determine as accurately as possible the Zener–Hollomon equation and its field of application, as well as to simulate a forging process whose characteristics are detailed below. These characteristics were determined arbitrarily to obtain specific results and they demonstrate the possibility of obtaining those results in a way which is not the only one possible and which, in general, need not be the same as a traditional forging sequence applied to a specific part.

2. Initial austenitic grain size

The final structure sought in both steels had to be the

0022–2461

TABLE I Data of steel 38C2

Chemical analysis

C = 0.39%	Mn = 0.5%	Si = 0.22%	P = 0.021%
S = 0.034%	Cr = 0.50%	Al = 0.034%	Ti = 0.002%
V = 0.005%	Mo = 0.034%	Cu = 0.23%	Ni = 0.20%

Treatment applied

Preheating 1250 °C	Forging 1090 °C	Air cooling
Quenching 850 °C	Tempering 600 °C	

Characteristics after treatment

Hardness, H_v	254	Elongation (L_0 = 5)	16.5%
R_m	811 MPa	Striction	58.9%
$R_{0.2}$	483 MPa	ASTM grain size	9

Impact strength (Mesnager notch)

at − 20 °C	120 J cm^{-2}
at 20 °C	121 J cm^{-2}

TABLE II Chemical composition (wt %)

	40MVS6	30MSiV62
C	0.39	0.29
Mn	1.29	1.30
Si	0.22	0.43
S	0.073	0.026
P	0.014	0.019
V	0.10	0.11
Al	0.020	0.029
N_2	70 p.p.m.	164 p.p.m.

finest ferrite–pearlite possible. As already mentioned in Section 1, this structure would be conditioned by two phenomena: the first of them, specific to steels subjected to high strains, was dynamic recrystallization, which occurs when a certain strain level is exceeded, to be examined later, and that due to the austenitic grain size, which is more important at lower strain levels. First of all this initial size was examined on test pieces of both steel (diameter = 2 mm, L = 12 mm) subject to heating rates of $v = 5\,^{\circ}C\,s^{-1}$ with a maintenance time at the maximum temperature of 120 s and a cooling rate of $v = 200\,^{\circ}C\,s^{-1}$.

Fig. 1 shows the results in terms of the different maintenance temperatures of the two steels.

Duplex grains were observed in the 30MSiV62 steel, with a maximum detected size difference 4–8 ASTM at 1050 °C. The same did not occur with the 40MVS6 steel, whose grain growth was more regular, although below the 1050 °C temperature the 30MSiV62 steel had a finer grain due to its higher nitrogen content which allowed for the formation of more vanadium precipitates.

3. Study of the treatment temperatures

Given that one of the objectives of this paper was energy saving, the temperature of each step taken was determined by the minimum values at which the

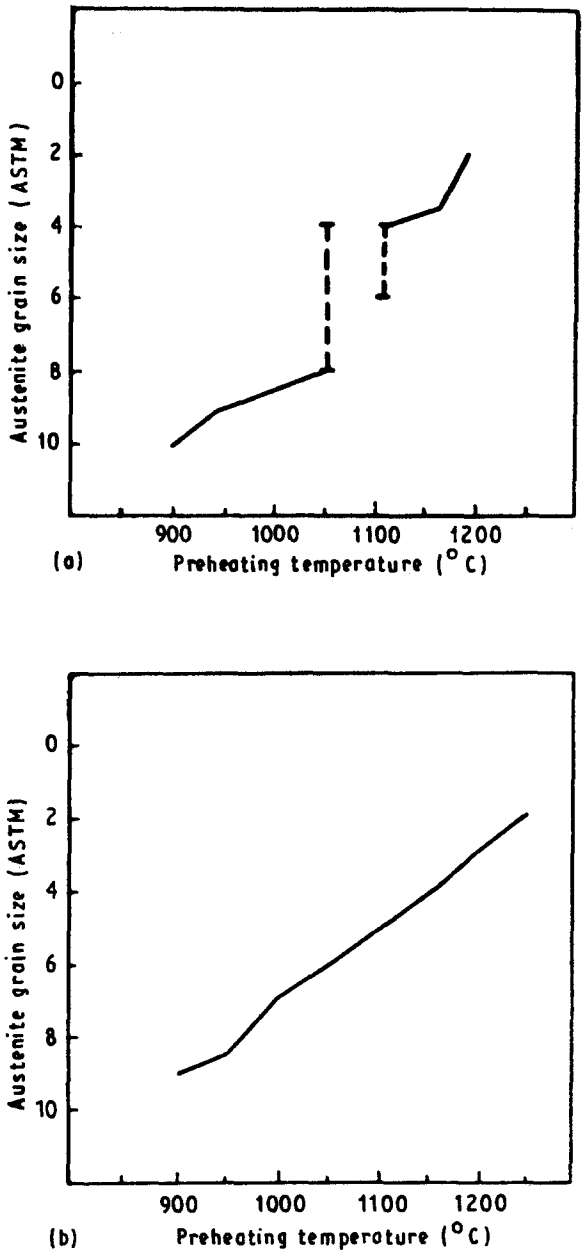

Figure 1 Relationship between undeformed austenite grain size and preheating temperature for (a) 30MSiV62 and (b) 40MVS6.

optimum treatment conditions were obtained, which in this type of steel are, on the one hand, the formation of precipitates and, on the other, maximum ductility.

The formation of specific precipitates: vanadium nitrides (VN), vanadium carbides (VC) and vanadium carbonitrides (VCN) acted specifically, adding its effects to those common to all aluminium-killed steels, slowing down recrystallization, inhibiting growth of the austenitic grain, refining the ferrite and producing hardening by precipitation. The solution of these carbides, which are typical of microalloyed steels, had thus to be obtained with an appropriate preheating temperature.

The solution temperatures of the VC and VN were calculated using the expressions

$$\log[V][C] = -\frac{9500}{T} + 6.72 \quad (1)$$

$$\log[V][N] = -\frac{8330}{T} + 3.46 \quad (2)$$

where [V] is the % by weight of vanadium, [C] the % by weight of carbon, [N] the % by weight of nitrogen, and T the preheating temperature (K). Table III is obtained from Equations 1 and 2, which established one of the minimums sought at 986 and 1070 °C, namely the preheating phase minimum, undoubtedly lower than the normal preheating temperatures in forging (1250 °C) as seen in Table I.

The second minimum sought directly determined the values of the forging processes temperature and was determined by the temperature providing a sufficient ductility to the material, in the forging conditions to which it was to be subjected, temperatures, strain and strain rate. To calculate them, the Stahl–Eisen standard [2] was followed, applied to the two-run forging of a car connecting rod such as the one manufactured with steel 38C2 of Table I, and the expression used was

$$\varepsilon = \ln \frac{h_0}{h} \tag{3}$$

$$\dot{\varepsilon} = \ln \frac{\varepsilon}{\Delta h} V_m \tag{4}$$

where h_0 is the initial height, h the final height, V_m the average velocity of the hammer from the beginning to the end of the strain, ε the average strain, and $\dot{\varepsilon}$ the average strain rate, from which the parameters of Table IV were obtained.

The equivalent magnitudes applicable in the torsion simulation were obtained from the expressions

$$\varepsilon = \left(\frac{2\pi R}{L\, 3^{\frac{1}{2}}}\right) N \tag{5}$$

$$\dot{\varepsilon} = \left(\frac{2\pi R}{L\, 3^{\frac{1}{2}}}\right) \dot{N} \tag{6}$$

where ε is the average strain, $\dot{\varepsilon}$ the average strain rate, R the test piece radius (mm), L the test piece length (mm), N the number of turns, and $\dot{N}$ the number of turns per second, which in line with the dimensions of the test piece and the data shown in Table IV for the first run gave $N = 6.6$ turns and $\dot{N} = 2000$ r.p.m., and for the second $N = 3.6$ turns and $\dot{N} = 2000$ r.p.m. Once the tests had been carried out at different temperatures, these data allowed Fig. 2 to be obtained. In accordance with these curves, the maximum ductility of the 40MVS6 steel was observed at 1200 °C, while in the 30MSiV62 steel this was at 1050 °C. However, both displayed a good plastic behaviour over a wide range of temperatures, which was larger in the 30MSiV62 steel.

The 30MSiV62 steel was later considered in this particular case to be more suitable, this decision being based on structural and hardness aspects marked by the steel to be substituted. Ductility tests were therefore conducted at other strain rates, which could represent other forging processes. The results are shown in Fig. 3.

A slight displacement of the maximum ductility zone towards higher temperatures was observed at 1100 and 1150 °C, together with a drop in the number of turns causing the breakage of the material, although the strain in each case remained invariable, around $\varepsilon = 17$–19. From 925 °C on, values of ε of over 8 were obtained, which easily exceeded those of any forging process.

TABLE III VC and VN solution temperatures in the steels under study

	40MVS6	30MSiV62
[V][C]	896 K	883 K
[V][N]	986 K	1070 K

TABLE IV Strain parameters used in simulation of a forging process

Run	Forging		Torsion	
	ε	$\dot{\varepsilon}$ (s^{-1})	N	$\dot{N}$ (r.p.m.)
1	1.443	7.25	6.6	2000
2	0.779	7.25	3.6	2000

4. Forging sequences

Once the minima of the different steps of the forging

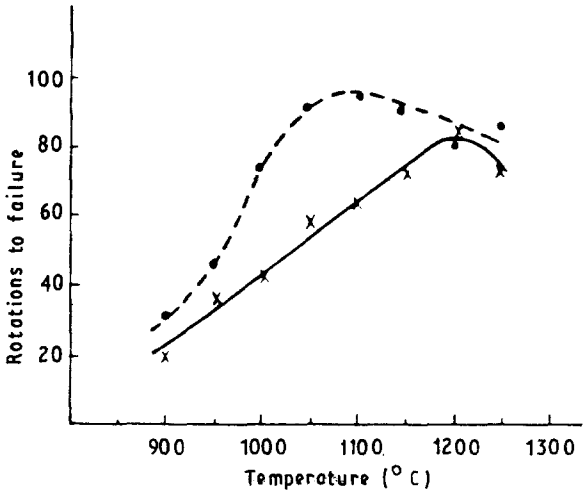

Figure 2 Ductility curves for (——) 40MVS6, and (– – –) 30MSiV6; $\bar{\dot{\varepsilon}} = 7.25\ s^{-1}$.

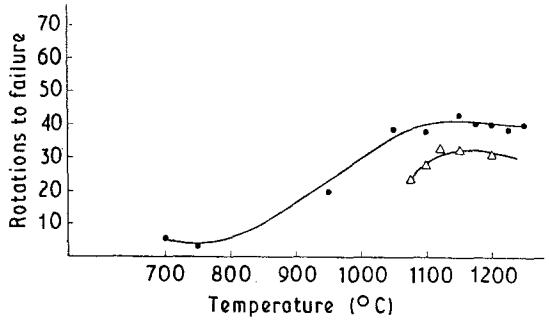

Figure 3 Ductility curves of 30MSiV62 for $\dot{\varepsilon} = (\bullet)\ 14\ s^{-1}$, $(\triangle)$ $22\ s^{-1}$.

process had been established (preheating and forging), the different possible sequences were studied in order to select one of them, based on the results obtained.

Although, as pointed out in Section 1, the objective was not to repeat the process undergone by the Q + T steel, certain basic conditions imposed by the process had to be respected: two steps to attain the desired reduction and an acceptable staggering of temperatures for the industrial start up. The heating time was that necessary to homogenize the structure and to produce the solution of the carbides and nitrides, in line with the test piece dimensions; the time between test steps was 3 s, and cooling was by air.

The simulations conducted were those shown in Table V.

Rectifications 0.3 mm deep were made along the useful length of all the test pieces assayed, in order to analyse the corresponding microstructures and determine the grain sizes. The final microstructure of both steels in all the conditions assayed, was ferrite and pearlite.

The analysis of the torque curves versus number of turns (see Figs 4 and 5) showed that the strain in the first run ($\varepsilon = 1.443$, $N = 6.6$ turns) was sufficient to produce dynamic recrystallization in both steels, when the temperature at which that strain occurred was over 950 °C. Fig. 6 shows the strain values needed to obtain the state of equilibrium between hardening by strain and recrystallization, which is lower than that applied. The same did not occur with the second strain, which occurred at lower temperatures and above all with a strain ($\varepsilon = 0.779$, $N = 3.6$ turns) which, in general, did not allow for the maximum point of the strain torsion curve to be exceeded, so it may be assumed that the final structure observed was due to dynamic recrystallization of the first step and to the static nature of the cooling which followed the second step. However, if one compares these with the grain-size values of Fig. 1, it is seen that there was a notable refinement of the final structure.

In the values obtained for hardnesses, one notes that the 40MVS6 steel displayed higher values than those for the 30MSiV62 steel and, given that the aim was to substitute a specific steel, the 38C2, in a particular piece, for which a maximum post-treatment hardness of 278 H_v is requested by the manufacturer, here one should, in principle, opt for the higher suitability of the 30MSiV62 steel. That is why in future, as shown in the ductility study, more extensive tests will be

TABLE V Thermal parameters used in simulating the described forging process by torsion

	Preheating furnace temp. (°C)	1st deformation (°C)	2nd deformation (°C)	Post-deformation cooling	Final grain size (ASTM)[a]
40MVS6 steel	1250	1225	1180		4/5
		1190	1130		5
		1170	1120	air	5/6
		1120	1075		6
		1010	960		7
		980	930		8
	1200	1180	1130		6/7
		1150	1110		6/7
		1120	1080	air	7
		1000	960		7/8
		950	910		8
	1150	1130	1070		6/7
		1130	1055	air	7
		1080	1010		7/8
	1100	1090	1050	air	7/8
		1090	1000		7/8
30MSiV62 steel	1200	1175	1115		5/6
		1150	1055		6
		1055	1010	air	(9/10)
		1010	955		(9/10)
		960	905		(10)
	1150	1110	1060		7
		1060	1005	air	(9/10)
		1010	955		(9/10)
		955	900		(10)
	1100	1085	1055	air	(9/10)
		1060	1000		(10)
	1050	1040	1005	air	(10)

[a] The numbers shown in brackets correspond to the values of ferritic grain sizes. The rest, not shown in brackets, correspond to the size of austenitic grains determined due to the presence of ferrite at the grain boundary.

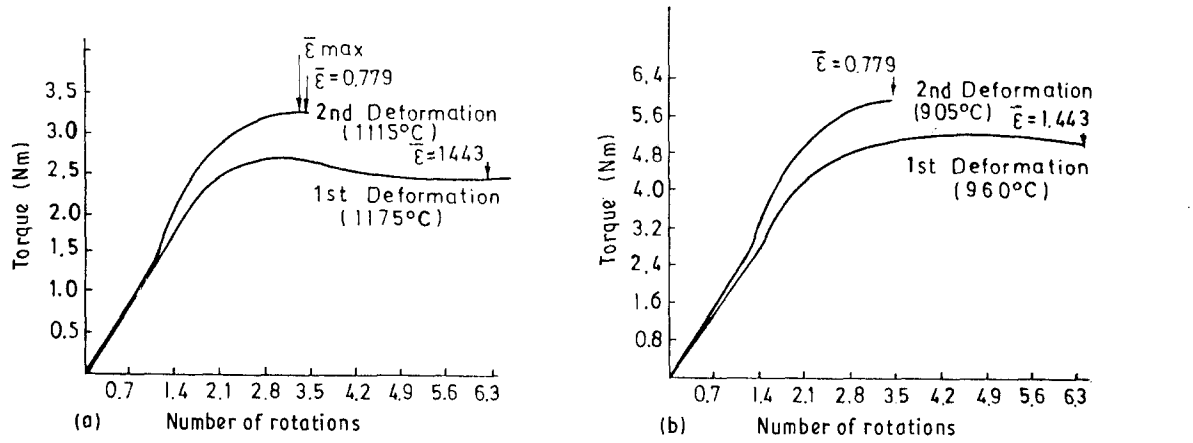

Figure 4 (a, b) Torque–number of rotations curves in two extreme temperatures of the last deformation for steel 30MSiV62. Preheating temperature 1200 °C, $\bar{\dot{\varepsilon}} = 7.25\ s^{-1}$.

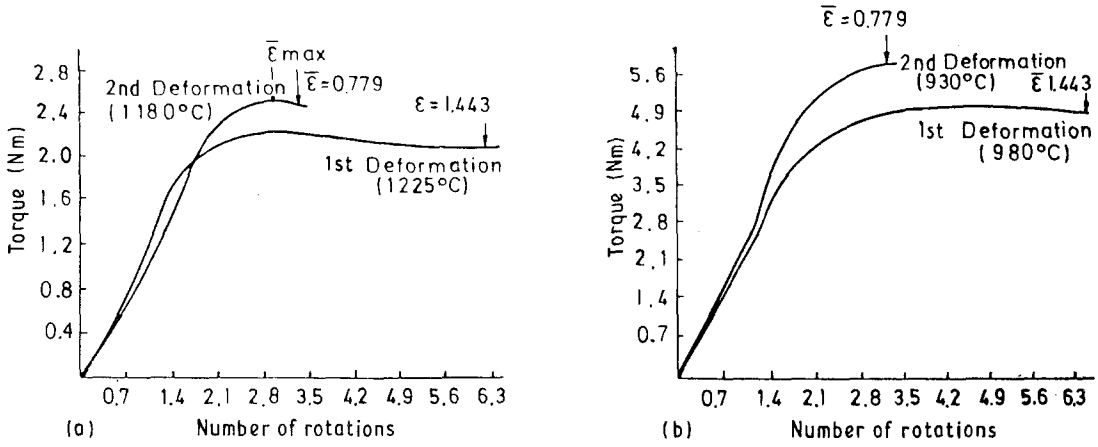

Figure 5 (a, b) As Fig. 4, for steel 40MVS6. Preheating temperature 1250 °C, $\bar{\dot{\varepsilon}} = 7.25\ s^{-1}$.

conducted on the second steel and the behaviour of the first will also be analysed, to provide sufficient data for other cases of substitution.

5. Strain parameters

Up to this point, the characteristics of both steels have been examined, reproducing the industrial start up conditions and for a specific process, a double upsetting whose two steps have the same strain rate, $\dot{\varepsilon} = 7.25\ s^{-1}$, and two different levels of strain, $\varepsilon = 1.443$ and 0.779. It might, however, be necessary to change some of the parameters utilized, due to manufacturing needs or conditions of use. Instead of repeating each and every one of the tests for each situation, the characteristics of the steel may be studied from a theoretical viewpoint, obtaining a state equation and, within margins specified later, theoretically obtain the conditions equivalent to the optimization conditions given so far. One of the various expressions proposed to express the dependence between stress, temperature and strain rate is the Zener–Hollomon function

$$Z = \dot{\varepsilon} e^{Q/RT} = A\,(\sinh \alpha\sigma_n)^n \qquad (7)$$

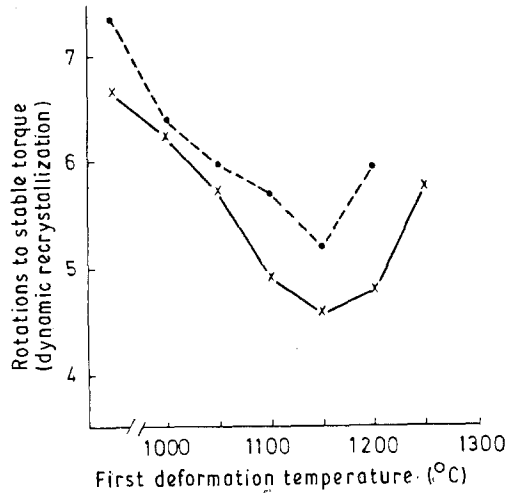

Figure 6 Relationship between first deformation temperature and number of rotations to stable torque (dynamic recrystallization) for (— × —) 40MVS6, (— ● —) 30MSiV62. $\bar{\dot{\varepsilon}} = 7.25\ s^{-1}$.

which is probably a more accurate description of the behaviour of the material in a wide range of T and $\dot{\varepsilon}$ values, where Z is the Zener–Hollomon parameter, $\dot{\varepsilon}$ the strain rate, Q the process activation energy, T the process temperature, R the perfect gases constant, A, α constants which only depend on the material, n a

constant of a value of around 5, and σ_n the saturation stress. This equation includes the concept of saturation stress, which is the stress corresponding to the stationary zone of the strain stress correspondence.

Given that until now the torque concept has only been mentioned in relation to the concepts of strain or strain rate, there now follows a brief study of the stress. Ample information as regards its theoretical basis may be found in the literature [3–5].

The effective stress of a torsion test is normally defined as

$$\sigma_s = \frac{3^{1/2}\Gamma}{2\pi R^3}\left[3 + \left(\frac{\delta \ln \Gamma}{\delta \ln \varepsilon}\right)_{\dot{\varepsilon}} + \left(\frac{\delta \ln \Gamma}{\delta \ln \dot{\varepsilon}}\right)_{\varepsilon}\right] \quad (8)$$

where Γ is the torque, R the test piece radius,

$$\left(\frac{\delta \ln \Gamma}{\delta \ln \varepsilon}\right)_{\dot{\varepsilon}} = n$$

a work-hardening exponent, and

$$\left(\frac{\delta \ln \Gamma}{\delta \ln \dot{\varepsilon}}\right)_{\varepsilon} = m$$

the strain rate sensitivity. To find the values of σ_s in terms of the torque one must therefore find the values of m and n of each test.

The values of n

$$n = \left(\frac{\delta \ln \Gamma}{\delta \ln \varepsilon}\right)_{\dot{\varepsilon}} = \left(\frac{\delta \ln \Gamma}{\delta \ln N}\right)_{\dot{N}} \quad (9)$$

were obtained for each temperature and each strain rate. In this case, the values obtained for $\dot{\varepsilon} = 7.25\ s^{-1}$ were those of Fig. 7. For $\dot{\varepsilon} = 0.725\ s^{-1}$ the value was practically zero, as may be deduced from Fig. 8.

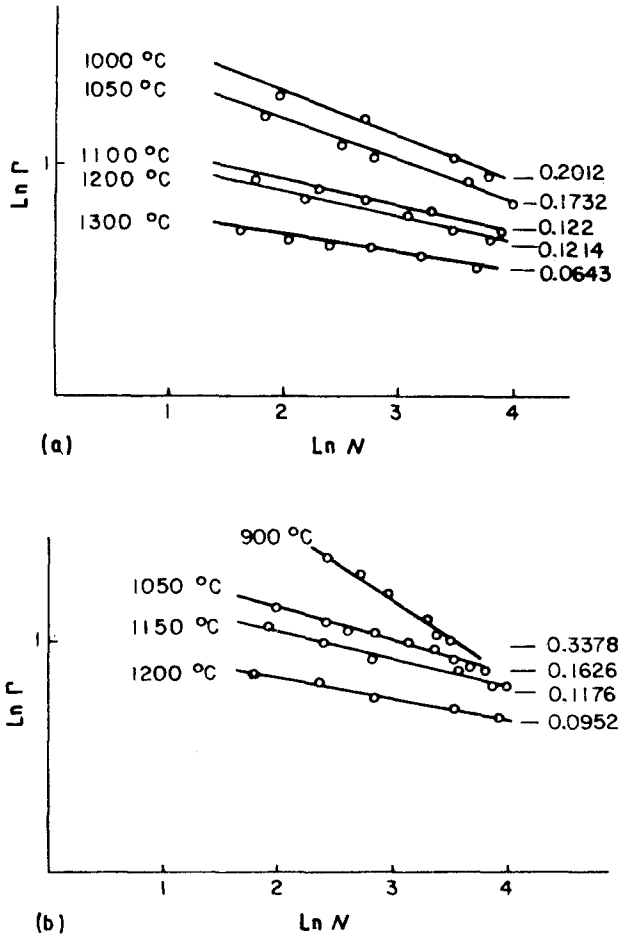

Figure 7 Work-hardening exponents, n, in (a) 30MSiV62, and (b) 40MVS6.

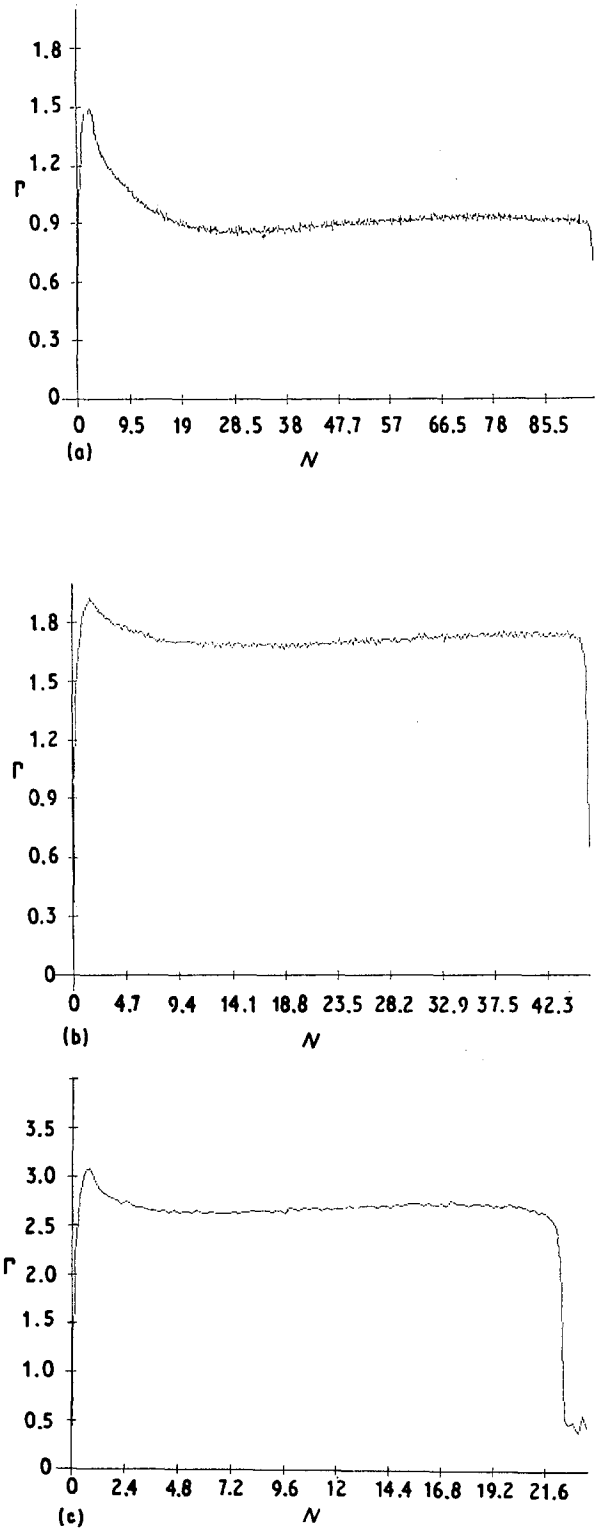

Figure 8 Γ–N relationship for $\dot{\varepsilon} = 0.725\ s^{-1}$, for (a) 40MVS6, (b) 30MSiV62, both at 1473 K, and (c) 30MSiV62 at 1323 K. Pass 1.

The values of m

$$m = \left(\frac{\delta \ln \Gamma}{\delta \ln \dot{\varepsilon}}\right)_{\varepsilon} = \left(\frac{\delta \ln \Gamma}{\delta \ln \dot{N}}\right)_{N} \quad (10)$$

were calculated from different strain rates and for a strain large enough for it to correspond to the stationary period of the effective stress ($\sigma_s = \sigma_n$). In the case of 30MSiV62 steel, $\varepsilon = 1.3$ equivalent to $N = 6$ turns and for 40MVS6 steel, $\varepsilon = 1.5$ equivalent to $N = 6.9$ turns.

The values obtained for the extreme magnitudes of the temperature are displayed in Fig. 9.

The function $\sigma = f(\varepsilon)$ was obtained as in Equation 8 and in Fig. 10 they are represented by both steels and $\dot{\varepsilon} = 7.25\ s^{-1}$.

Additional tests were conducted at different temperatures and strain rates.

We have represented the function $\sigma = f(\varepsilon)$ corresponding to 30MSiV62 steel for strain rate $\dot{\varepsilon} = 13.7\ s^{-1}$ and at different temperatures in Fig. 11. The values obtained for both steels are given in Tables VI and VII.

The values obtained were used to solve Equation 7 using the least squares method and 373 iterations, which give an error of 2.15%. Establishing the values of Q and $\dot{\varepsilon}$, the regression line was calculated

$$\ln Z = \ln A + n \ln(\sinh \alpha\sigma) \quad (11)$$

the results being for 30MSiV62 steel

$$\dot{\varepsilon} e^{60\,330/RT} = 1.015 \times 10^{11} (\sinh 0.0064\ \alpha\sigma)^{5.21} \quad (12)$$

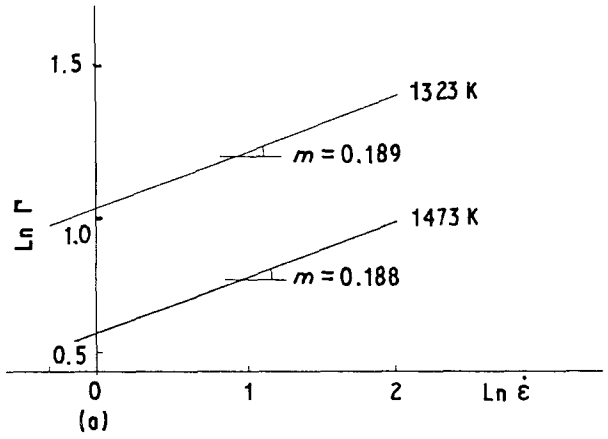

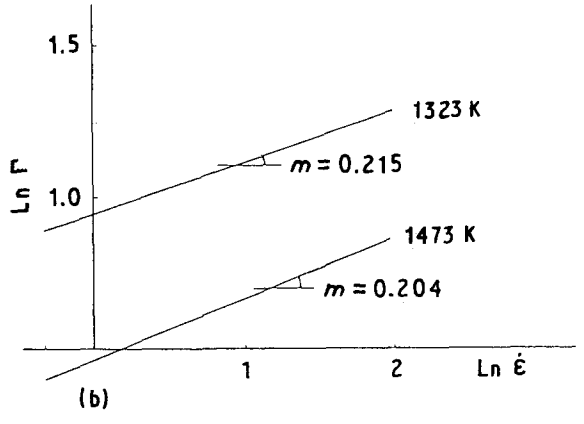

Figure 9 Strain-rate sensitivity in (a) 30MSiV62, $\varepsilon = 1.3$, (b) 40MVS6, $\varepsilon = 1.5$.

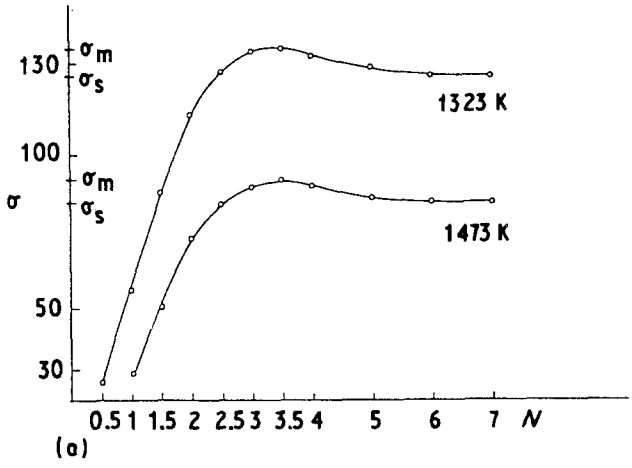

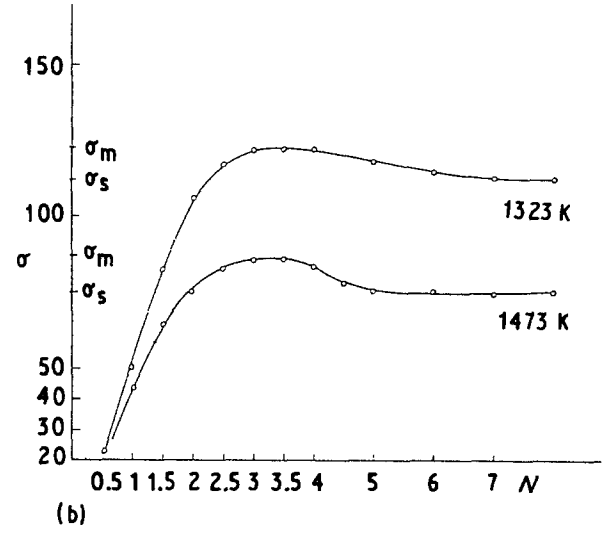

Figure 10 Stress–strain relations in (a) 30MSiV62, (b) 40MVS6. $\dot{\varepsilon} = 7.25\ s^{-1}$.

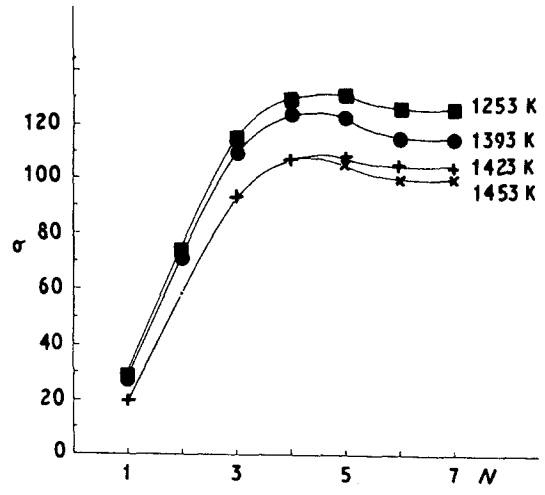

Figure 11 Stress–strain relations for 30MSiV62.

TABLE VI Parameters of the 30MSiV62 steel

$\dot{\varepsilon}$ (s^{-1})	1323 K	1353 K	1393 K	1423 K	1453 K	1473 K
0.725	$m = 0.189$ $n \simeq 0$ $\sigma_s = 85.6$ MPa					$m = 0.188$ $n \simeq 0$ $\sigma_s = 56$ MPa
1.37		$m = 0.189$ $n \simeq 0$ $\sigma_s = 87.8$ MPa	$m = 0.189$ $n \simeq 0$ $\sigma_s = 78.1$ MPa	$m = 0.187$ $n \simeq 0$ $\sigma_s = 74.2$ MPa	$m = 0.188$ $n \simeq 0$ $\sigma_s = 65.1$ MPa	
7.25	$m = 0.189$ $n = -0.1732$ $\sigma_s = 126$ MPa					$m = 0.188$ $n = -0.1214$ $\sigma_s = 84$ MPa
13.7		$m = 0.189$ $n = -0.22$ $\sigma_s = 127$ MPa	$m = 0.184$ $n = -0.17$ $\sigma_s = 115.6$ MPa	$m = 0.184$ $n = -0.154$ $\sigma_s = 105.3$ MPa	$m = 0.189$ $n = -0.123$ $\sigma_s = 100.0$ MPa	

TABLE VII Parameters of the 40MVS6 steel

$\dot{\varepsilon}$ (s^{-1})	1323 K	1423 K	1473 K
0.725	$m = 0.215$ $n \approx 0$ $\sigma_s = 80$ MPa		$m = 0.204$ $n \approx 0$ $\sigma_s = 49.5$ MPa
5.44	$m = 0.215$ $n = -0.16$ $\sigma_s = 105$ MPa	$m = 0.208$ $n = -0.106$ $\sigma_s = 82$ MPa	$m = 0.204$ $n = -0.089$ $\sigma_s = 69.3$ MPa
7.25	$m = 0.215$ $n = -0.1626$ $\sigma_s = 113$ MPa	$m = 0.208$ $n = -0.1176$ $\sigma_s = 82$ MPa	$m = 0.204$ $n = -0.0952$ $\sigma_s = 74$ MPa

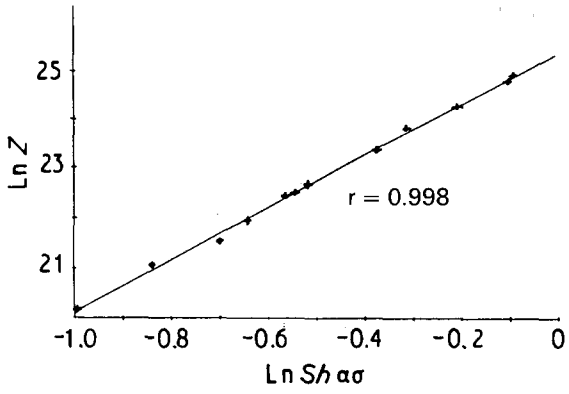

Figure 12 The Zener–Holloman equation for 30MSiV62.

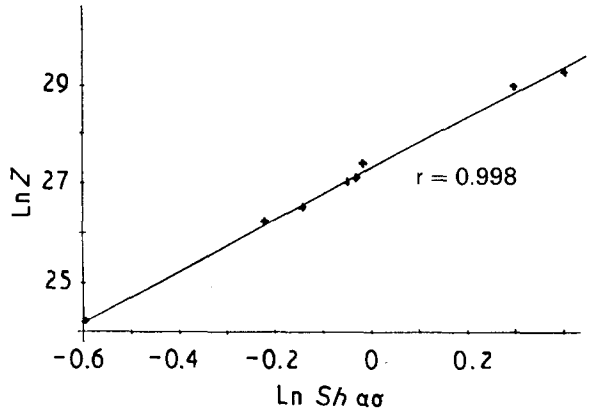

Figure 13 The Zener–Holloman equation for 40MSV6.

and for 40MVS6 steel

$$\dot{\varepsilon} e^{72\,210/RT} = 7.18 \times 10^{11} (\sinh 0.0106\ \alpha\sigma)^{5.14} \quad (13)$$

and representation of Equation 11 is that shown in Figs 12 and 13.

These equations are valid as long as the adiabatic heating does not distort the results. This occurs in torsion tests of over 1273 K and during forging at somewhat lower temperatures because there is greater thermal diffusion through the tool.

In the example studied, the creep value was only obtained for the stress in the 30MSiV62 steel and for the first strain in which $\varepsilon = 1.443$ exceeded the value $\varepsilon = 1.3$ obtained for σ_s. For this steel, taking into account the values permitted for the grain size, the conditions of $\dot{\varepsilon}$ and T could be varied according to the possibilities of the machinery in line with the Zener–Hollomon equation calculated, so that its Z parameter remains constant. For example, the conclusions recommend a preheating of 1100 °C and the first run at 1080 °C, which would give

$$Z = 7.25 e^{60\,330/2.1353} = 3.49 \times 10^{10} \quad (14)$$

If only a strain rate of $\dot{\varepsilon} = 6.5\ s^{-1}$ were attained,

forging would have to be conducted at a temperature fulfilling

$$Z = 6.5e^{60336/2T}$$

$$= 3.49 \times 10^{10}$$

$$T = 1346.4\,\text{K, i.e. } 1073.4\,^{\circ}\text{C}$$

Similarly, in other forging processes where the strains $\varepsilon = 1.3$ and 1.5 are exceeded, respectively, we could operate with the equations obtained.

6. Experimental data

This section refers to the 30MSiV62 steel, which is the most suitable for substituting the 38C2 in the case studied. The sequence process which, in accordance with the above sections, may be considered the most appropriate, was conducted, comprising preheating at 1100 °C (permitting the dissolution of carbides and nitrides), first blow at 1080 °C (permitting dynamic recrystallization), and the second blow at 1050 °C (limit for the appearance of duplex grain in static recrystallization).

The strain parameters were $\dot{\varepsilon} = 7.25\,\text{s}^{-1}$ in both blows and the strain was $\varepsilon = 1.433$ in the first and $\varepsilon = 0.779$ in the second step

The results obtained were $R_m = 874$ MPa, $R_{0.2} = 633$ MPa, $A = 18.5\%$, striction = 55.4%. Impact strength with Mesnager notch at 20 °C = 109 J cm^{-2}, and at − 20 °C = 107 J cm^{-2}, and the metallographic structure corresponded to that of Fig. 14a, where one may also observe a micrograph of the structure obtained in the 38C2 after Q + T, Fig. 14b.

This steel gave good results because although the impact strength results were lower, they were within the conditions of use accepted by the manufacturer.

7. Conclusions

In general terms, it may be said that both steels can be used to substitute other Q + T steels in the hot forging processes, although in this particular case and given the characteristics of the part to be manufactured, one should opt for the 30MSiV62 steel whose final mechanical and structural properties are better suited to the manufacturer's conditions. In particular, the 40MVS6 steel is excluded as a result of the final hardness required for the part studied. Nevertheless, some general remarks may be made as regards the utilization of both steels and each particular problem leads us to choose one or other of the two or to commence a complementary study.

The wide range of temperatures over which these two steels displayed a high ductility allowed for the temperatures to be adapted to those to which it was possible to apply the series of strains, in order to attain in the material, directly from forging, the final structure most suited to the requirements for each application, without the need for later costly heat treatments.

Focusing simply on structural observations, from the appraisal of the results given in this report it may be concluded that in both steels the best microstructure was obtained when the final strain of the process took place at lower temperatures. In these conditions,

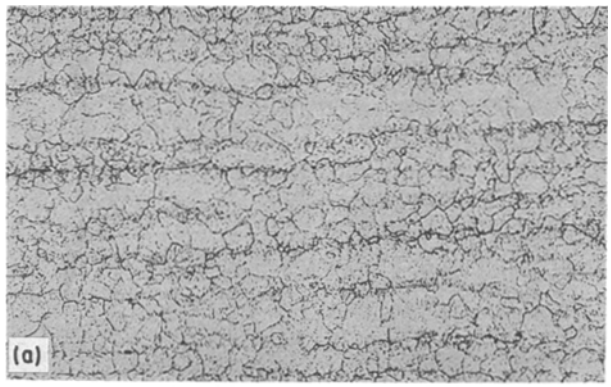

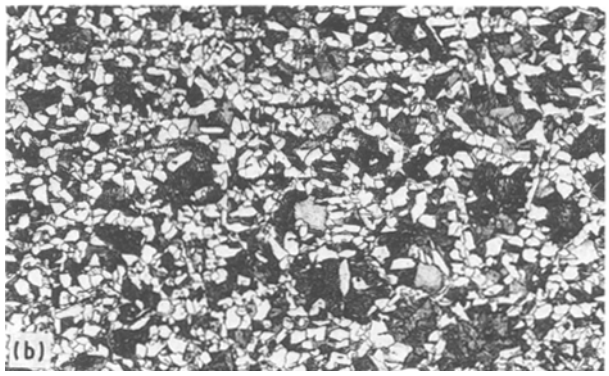

Figure 14 Microstructure of steel (a) 38C2, Q + T and (b) 30MnSiV62 after forging. Magn × 200.

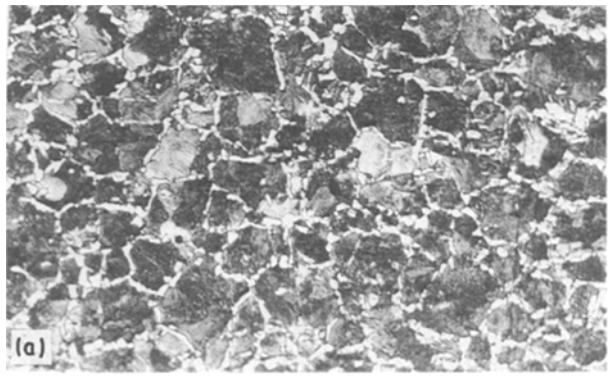

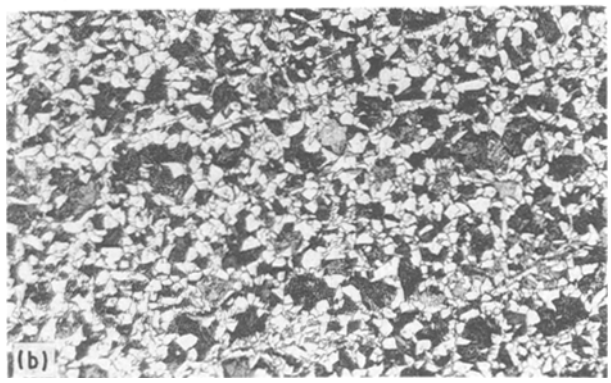

Figure 15 Microstructure of steel (a) 40MVS6 and (b) 30MSiV62 in the same condition. Magn × 200.

later air cooling generated fine-grain ferritic–pearlitic microstructures. In this respect, the higher level of nitrogen in the 30MSiV62 steel allowed for the formation of larger amounts of precipitates, which in turn resulted in this steel having a considerably finer grain

size than the 40MVS6 steel for the same temperature cycles associated with strain.

Fig. 15 shows micrographs of both steels subjected to the same forging process: preheating temperature 1200 °C; first run temperature ($\varepsilon = 1.433$) 1060 °C; second run temperature ($\varepsilon = 0.779$) 1010 °C; strain rate in both runs 7.25 s^{-1}, and air cooling under the same conditions. In these micrographs one may observe the different grain sizes of both steels, 7 ASTM for 40MVS6 (Fig. 15a) and 9/10 ASTM for the 30MSiV62 (Fig. 15b), as well as the precipitation of proeutectoid ferrite at grain edges produced in the first steel. Although this type of microstructure may reduce the impact strength of this material, its acceptable grain size obtained by cooling directly from forge makes this steel a possible substitute for many heat-treated alloy steels. Beyond all doubt is the case of 30MSiV62 steel which, with a ferritic–pearlite structure with grain sizes of 9 or 10 ASTM and a fine pearlite structure, guaranteed impact strength, elastic limit and resistance properties levels. It can thus substitute many alloyed steels in the Q + T state, with considerable economic advantages.

The experimental results also showed that the preheating temperature had no notable influence on the final microstructure and grain size, which depended exclusively on the strain temperatures when all other parameters were equal (size of the strain in runs, strain rate, time between runs and post-forging cooling rates).

Consequently, because the solubilization of precipitates was ensured in these steels from sufficiently low temperatures (986 °C for 40MVS6 and 1070 °C for 30MSiV62), the use of preheating temperatures lower than those normally used in forging would result in considerable additional advantages, apart from the obvious energy savings. In the forging process itself, the possibility of reducing the preheating temperatures is a factor which plays a large part in prolonging the life of the matrices.

All these reasons point to the suitability of forging these steels at the lowest temperatures possible. Nonetheless, it would seem that the preheating temperature should not be lower than 1100 °C, nor should the temperature of the last strain be lower than 1000 °C. In both cases, the action of the microalloys could be less effective and the operational difficulties of the process would increase considerably.

Following on from this, it may be concluded that the best forging process for these microalloyed steels, considered an authentic thermomechanical treatment, should take place under the following conditions. For the 40MVS6 steel, which displays a maximum ductility temperature at 1200 °C, which remains high from 1000 °C, a regular austenitic grain growth, a precipitate solubilization temperature close to 1000 °C and a minimum temperature to produce incipient dynamic recrystallization in the second strain ($\varepsilon = 0.779$), the most suitable thermomechanical treatment for the manufacturing of a part from this steel, with the strain parameters used in this report, could take place under the conditions: preheating temperature 1150 °C, first strain temperature 1120 °C, second and last strain temperature 1090 °C, air cooling immediately after the last strain at rates of between 50 and 250 °C min^{-1}. Under these conditions, the final steel microstructure will be ferritic–pearlite with a 6 or 7 ASTM grain size, depending on the post-forging cooling rate applied.

For 30MSiV62 steel, whose maximum ductility is at 1100 °C, which remains high from 950 °C, a rapid grain growth temperature from 1050 °C, a total precipitate solubilization temperature of 1070 °C and a minimum temperature of 1070 °C to produce incipient dynamic recrystallization in the second strain ($\varepsilon = 0.779$), the most suitable thermomechanical treatment for the manufacturing of a part from this steel, with the strain parameters used in this report, could be: preheating temperature 1100 °C, first strain temperature 1080 °C; second and last strain temperature 1050 °C, and air cooling immediately after the last strain at rates of between 50 and 250 °C min^{-1}. Under these conditions, the 30MSiV62 steel will have a very fine pearlite and ferrite microstructure (9/10 ASTM) of high mechanical characteristics.

Evidently the decision to reduce the temperatures of the forging process of these steels requires suitable control of all the strain and thermal parameters and necessarily involves serious reconsideration of certain operational and design aspects which would be affected by this decision.

References

1. T. GLADMAN, Proceedings of "Information Day on Microalloyed engineering steels", Düsseldorf, June 30 (1988).
2. Stahl–Eisen Standard *Prufblatter* (*SEP* 1123) *des Vereins Deutscher Eisenhüttenleute*, Verlag Stahleisen, RFA, September (1986) 112.
3. J. J. URCOLA GALARZA and M. FUENTES PÉREZ, *Rev. Metal. CENIM* **16** (1980) 337.
4. H. OSUZU, T. SHIRAGA, K. TSUJIRUMA, Y. SHIROI, Y. TANIGUCHI and H. KIDO, SAE Technical Paper Series 860131 (Society of Automotive Engineers Inc., USA 1986).
5. G. PIERSON, G. METAEUR and M. GANTOIS, *Mem. Etude Sci. Rev. Metall.* May (1984) 239.
6. L. BACKER and J. FOMBARLET, *Aciers Speciaux* **72** (1985) 21.
7. C. GARCÍA, M. CARSÍ, S. F. MEDINA and M. P. DE ANDRÉS, in "World Material Congress", Conference Proceedings (ASM, Metals Park, OH, 1988) pp. 471–9.
8. C. GARCÍA, M. P. DE ANDRÉS, S. F. MEDINA and M. CARSÍ, "Jornadas Nacionales de Calidad Siderúrgica '85" (UNESID, 1985).
9. V. OLLILAIMEN, H. HURMOLA and H. PONTINEN, *J. Mater. Energy Systems* **5** (1984) 222.

Received 9 July 1990
and accepted 6 February 1991